

Observed Linkages between the Northern Annular Mode/North Atlantic Oscillation, Cloud Incidence, and Cloud Radiative Forcing

Ying Li and David W. J. Thompson

*Department of Atmospheric Science, Colorado State University
Fort Collins, Colorado, U.S.A.*

Yi Huang and Minghong Zhang

*Department of Atmospheric and Oceanic Sciences, McGill University
Montreal, Quebec, Canada*

1. Introduction

The northern annular mode/North Atlantic Oscillation (NAM/NAO) is the dominant pattern of climate variability in the Northern Hemisphere extratropical circulation (*e.g.*, Hurrell 1995; Thompson and Wallace 2000; Hurrell *et al.*, 2003). The NAM/NAO is associated not only with significant changes in the zonal wind but also in the mean meridional circulation and thus presumably the vertical structure of cloud incidence. The objective of this study is to examine and interpret the signature of the NAM/NAO in the horizontal and vertical structures of cloud incidence and cloud radiative forcing using nearly five years of CloudSat/CALIPSO data.

2. Data and methodology

2.1 Data

We use the cloud fraction data obtained from the combined radar and lidar retrievals 2B- GEOPROF-LIDAR product (version P2R04; Mace *et al.* 2009). The results are presented in terms of “cloud incidence”, which provides a quantitative estimate of the likelihood of a cloud within a given volume sensed by the satellite (Verlinden *et al.*, 2011; Li and Thompson 2013; Li *et al.* 2014). The analyses here are based on ~5 years of CloudSat observations from June 2006 through April 2011.

Various fields are also derived from monthly-mean output from the European Centre for Medium Range Weather Forecasts (ECMWF) Interim Reanalysis (ERA-Interim) (Simmons *et al.* 2007). The ERA-Interim is used to calculate the surface temperature, atmospheric temperature, specific humidity, surface albedo, top of the atmosphere (TOA) radiation fluxes anomalies associated with the NAM/NAO. It is also used to supplement the satellite derived cloud incidence.

2.2 Decomposition of radiation anomalies associated with NAM/NAO

We apply the radiative kernel method (Huang *et al.* 2007; Soden *et al.* 2008; Shell *et al.* 2008) to diagnose variations in TOA radiative fluxes associated with the NAM/NAO. The longwave radiative flux anomalies are decomposed into contributions from changes in surface and atmospheric temperature, atmospheric water vapor, and cloud; the shortwave radiative flux anomalies are decomposed into contributions from changes in surface albedo, atmospheric water vapor, and cloud.

Taking the longwave radiation anomalies as an example, the clear- and all-sky anomalies are decomposed as:

$$\Delta R^{clear} = \Delta R_T^{clear} + \Delta R_q^{clear} + Z^{clear} \quad (1)$$

$$\Delta R^{all} = \Delta R_T^{all} + \Delta R_q^{all} + \Delta R_{cloud} + Z^{all} \quad (2)$$

where ΔR denotes the TOA longwave radiation anomalies associated with the NAM/NAO, ΔR_T , ΔR_q and ΔR_{cloud} represent contributions from change in surface and atmospheric temperature, atmospheric water vapor, and cloud, respectively. Z is the residual term, which provides a measure of the fidelity of the linear decomposition assumption.

The non-cloud contributions are calculated as follows:

$$\Delta R_T = \frac{\partial R}{\partial T} \Delta T; \quad \Delta R_q = \frac{\partial R}{\partial q} \Delta q \quad (3)$$

where $\frac{\partial R}{\partial T}$ and $\frac{\partial R}{\partial q}$ are the pre-calculated global radiative kernels based on the Geophysical Fluid Dynamics Laboratory (GFDL) general circulation model (GCM) (Soden *et al.* 2008); ΔT and Δq correspond to regression anomalies in surface and atmospheric temperature and atmospheric water vapor, respectively, associated with the NAM/NAO.

The cloud contribution is derived by combining equations (1) and (2):

$$\begin{aligned} \Delta R_{cloud} &= (\Delta R^{all} - \Delta R^{clear}) - (\Delta R_T^{all} - \Delta R_T^{clear}) - (\Delta R_q^{all} - \Delta R_q^{clear}) \\ &= (\Delta R^{all} - \Delta R^{clear}) - \left(\frac{\partial R^{all}}{\partial T} - \frac{\partial R^{clear}}{\partial T} \right) \Delta T - \left(\frac{\partial R^{all}}{\partial q} - \frac{\partial R^{clear}}{\partial q} \right) \Delta q \end{aligned} \quad (4)$$

Note that the cloud radiative forcing (CRF) is defined as the difference between all- and clear- sky radiative anomalies ($CRF \equiv \Delta R^{all} - \Delta R^{clear}$) so that ΔR_{cloud} obtained by adjusting the CRF for the impacts of changes in T and q is often referred to as *adjusted CRF* (Shell *et al.* 2008; Soden *et al.* 2008).

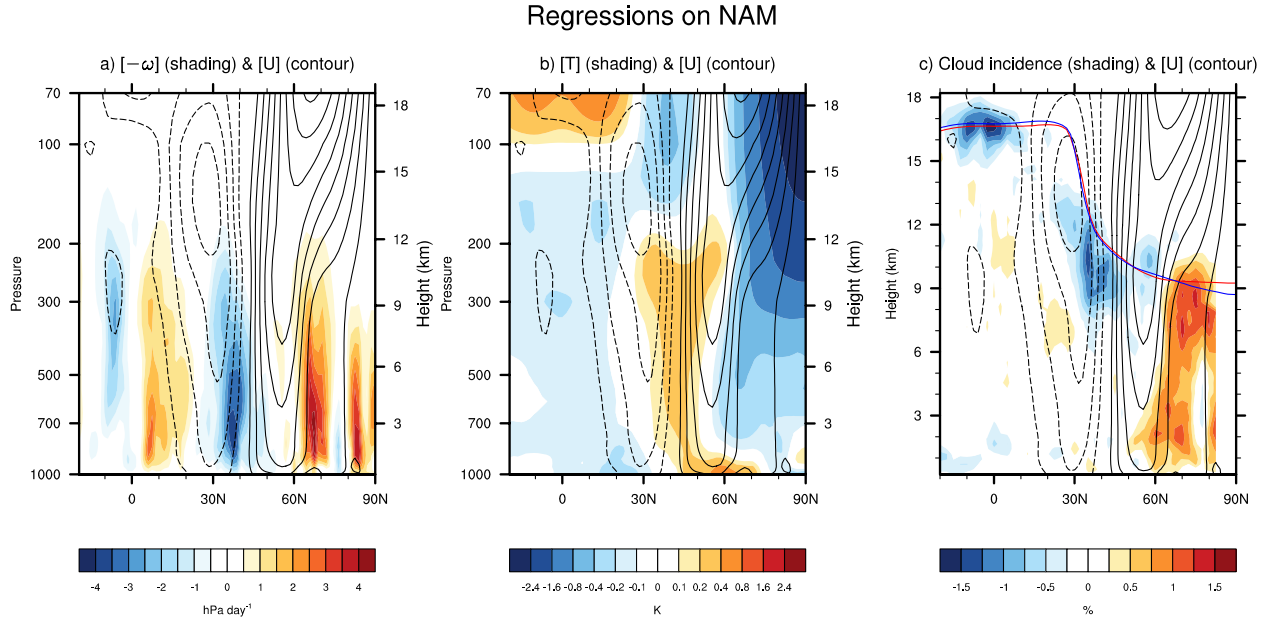


Fig. 1 Regressions of zonal-mean (a) pressure vertical motion (shading; ω has been multiplied by -1 so that positive values correspond to upward motion) and zonal wind (contour), (b) temperature (shading) and zonal wind (contour), and (c) cloud incidence (shading) and zonal wind (contour) onto standardized monthly-mean values of the anomalous NAM/NAO index. Results are based on October–March data from June 2006–April 2011. The seasonal cycle has been removed from the data. Units are K (temperature), hPa day⁻¹ (pressure vertical motion) and % (cloud incidence). Contour interval of zonal wind is 0.5 m s⁻¹ (dashed contours indicate negative values). The red and blue lines in (c) indicate the climatological-mean tropopause height plus and minus the regression of tropopause height onto the standardized NAM/NAO index, respectively. Tropopause height is identified using the WMO lapse rate definition.

3. Results

3.1. Zonally averaged circulation

Figure 1 reviews key aspects of the signature of the NAM/NAO in the zonal-mean circulation (Figs. 1a and b), and corresponding changes in cloud incidence (Fig. 1c). The positive polarity of the NAM/NAO is characterized by increases in zonally averaged cloud incidence north of $\sim 60^\circ\text{N}$, decreases between $\sim 25\text{--}50^\circ\text{N}$, and increases in the subtropics (Figure 1c). For the most part, the largest anomalies in upper tropospheric cloud incidence coincide with the largest changes in vertical motion: downward anomalies in vertical motion at middle latitudes overlie decreases in cloud incidence; upward anomalies in vertical motion at high latitudes overlie increases in cloud incidence.

Figure 2 quantifies the zonal-mean downwelling TOA longwave radiation anomalies associated with the NAM/NAO. The very close agreement between the solid (calculated directly from the ERA-Interim reanalysis) and dashed lines (calculated from radiative kernel method) in panel a and c indicates that the residual terms in equations (1) and (2) are very small, and thus that the linear decomposition of TOA radiation

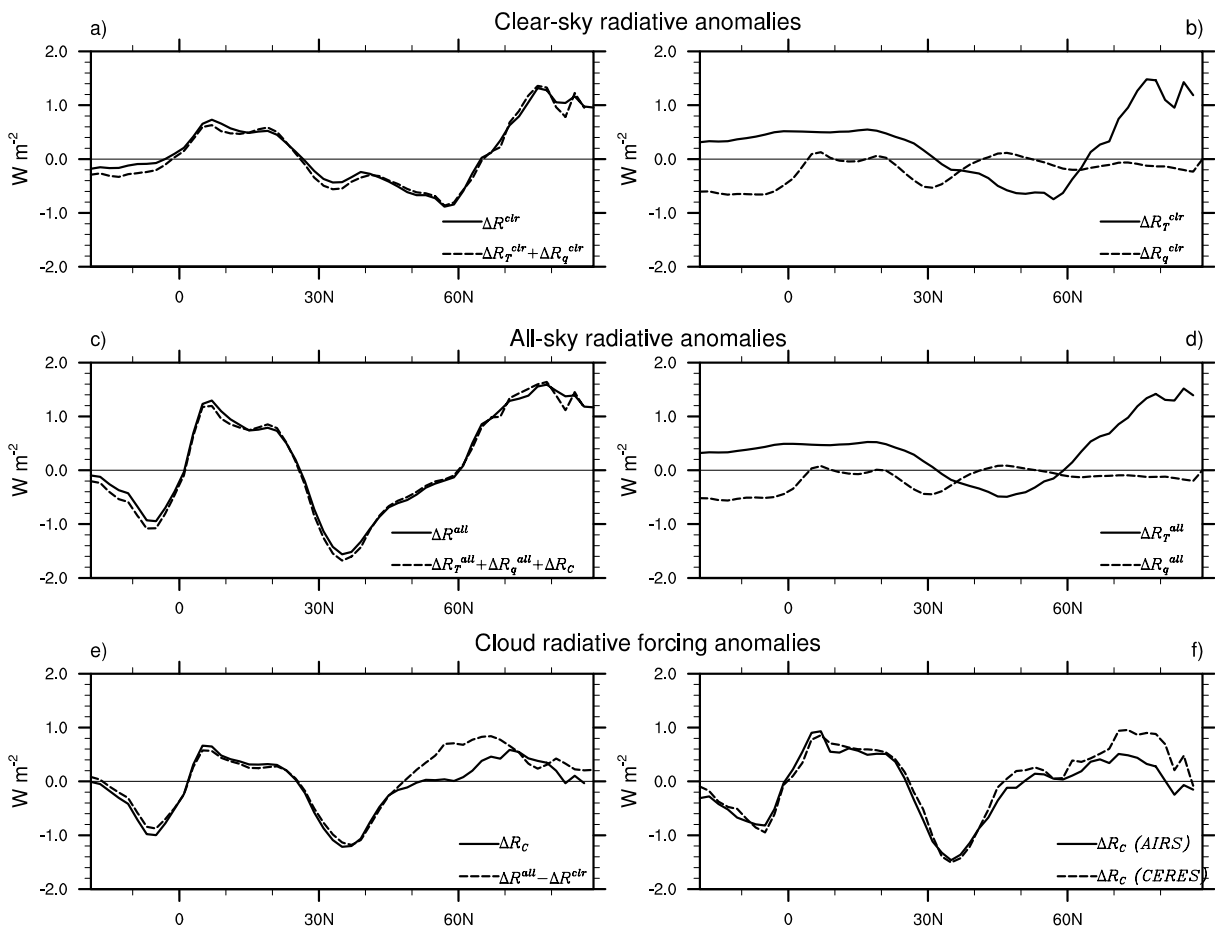


Fig. 2 (a) Zonal-mean TOA downwelling longwave clear-sky radiation anomalies associated with the NAM/NAO calculated directly from the ERA-Interim reanalysis (solid line) and derived from the sum of the contributions from various physical factors using the radiative kernel method (see Eq. 1; dashed line). (b) downwelling longwave radiation anomalies contributed from changes in temperature (solid line) and water vapor (dashed line). (c)-(d) As in (a)-(b), but for all-sky conditions. (e) adjusted cloud radiative forcing (CRF) estimated using the radiative kernel method [solid line, see Eq. 4], and CRF anomalies estimated as the simple difference between the all- and clear-sky radiative fluxes (dashed line). (f) adjusted CRF based on AIRS (solid line) and CERES EBAF (dashed line) observations.

anomalies by the kernel method is robust. The non-cloud contributions to the net changes in longwave forcing are dominated by the changes in surface and atmospheric temperature (solid lines in panels b and d).

Figure 2e shows the changes in longwave CRF (dashed) and adjusted longwave CRF (solid) associated with variability in the NAM/NAO. Both results indicate: 1) longwave warming due to clouds north of $\sim 60^\circ\text{N}$, where the NAM/NAO is associated with increases in cloud incidence; and 2) longwave cooling due to clouds between $\sim 25\text{--}50^\circ\text{N}$, where the NAM/NAO is associated with decreases in cloud incidence. The difference between the two longwave estimates within the latitude band $\sim 50\text{--}70^\circ\text{N}$ is centered over Northern Eurasia (not shown), where the large surface warming associated with the NAM/NAO is accompanied by strong cooling in the troposphere, and thus a large increase in the temperature lapse rate. As noted in Huang and Ramaswamy (2009), such a large change in the lapse rate may be mistaken for a cloud radiative effect in simple differences between all- and clear-sky radiation.

3.2 North Atlantic sector

Variations in the NAM/NAO are marked by a range of cloud incidence anomalies over the North Atlantic sector. A key result of Figure 3 is that the changes in upper tropospheric cloud incidence indicated by CloudSat are reproducible in the ERA-Interim reanalysis (compare Figure 3b and 3c), and they are qualitatively consistent with the attendant changes in anomalous vertical velocity (compare Figure 3a and 3b).

Figure 4 shows the geographical distribution of the downwelling TOA radiation anomalies associated with the NAM/NAO. The large contributions of the TOA longwave radiation anomalies due to changes in surface and atmospheric temperature are found over the continental areas, and are consistent with the negative Planck and lapse rate feedbacks.

The longwave cooling due to clouds peaks in a region extending eastward from the east coast of the U.S. to eastern Europe (Figure 4b), and is coincident with the decreases in high cloud incidence found over those locations (Figures 3b, c). The longwave warming due to clouds peaks over the subtropical North Atlantic and the subpolar North Atlantic (Figure 4b), and is coincident with the increases in high cloud incidence found over those regions (Figures 3b, c). The spatial consistency between the longwave adjusted CRF and the anomalous high cloud incidence from two independent datasets further corroborates the robustness of our estimate of variations in cloud radiative forcing due to variability in the NAM/NAO.

The shortwave adjusted CRF is negligible over high latitudes where the incident solar radiation is very weak during winter. Over the North Atlantic mid/low latitudes, the shortwave adjusted CRF is still a factor of 2–3 smaller in magnitude than that due to the longwave forcing. Thus, the total adjusted CRF associated with the NAM/NAO is dominated by the longwave component (Figure 4c).

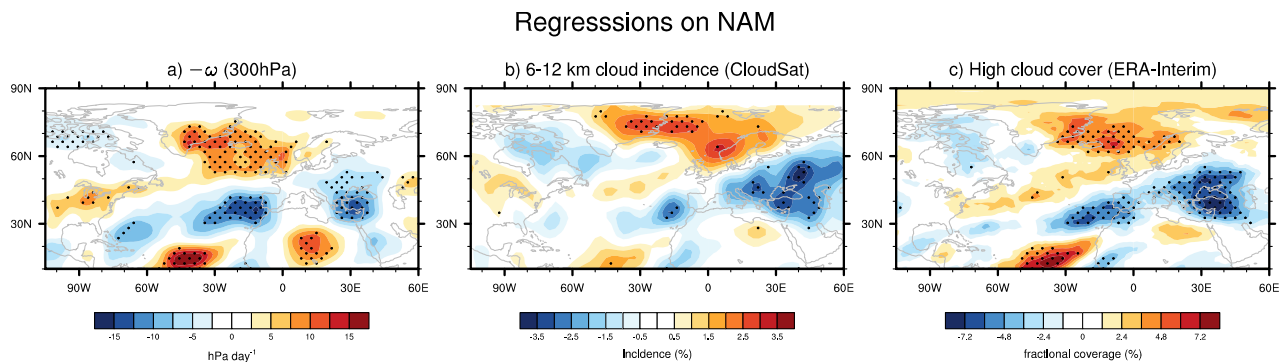


Fig. 3 Regressions of monthly-mean (a) pressure vertical motion (upward motion is positive) at 300 hPa, (b) cloud incidence averaged between 6–12 km based on CloudSat/CALIPSO dataset and (c) high-cloud fractional coverage based on ERA-Interim reanalysis onto standardized monthly-mean values of the anomalous NAM/NAO index. Stippling indicates results that exceed 95% confidence level based on a two-tailed test of the t-statistic, with the effective degrees of freedom computed given by equation (31) in Bretherton *et al.* (1999). The results in (a) and (b) have been smoothed with a NCAR Command Language (NCL) built-in 9-point smoothing function for the purpose of display only.

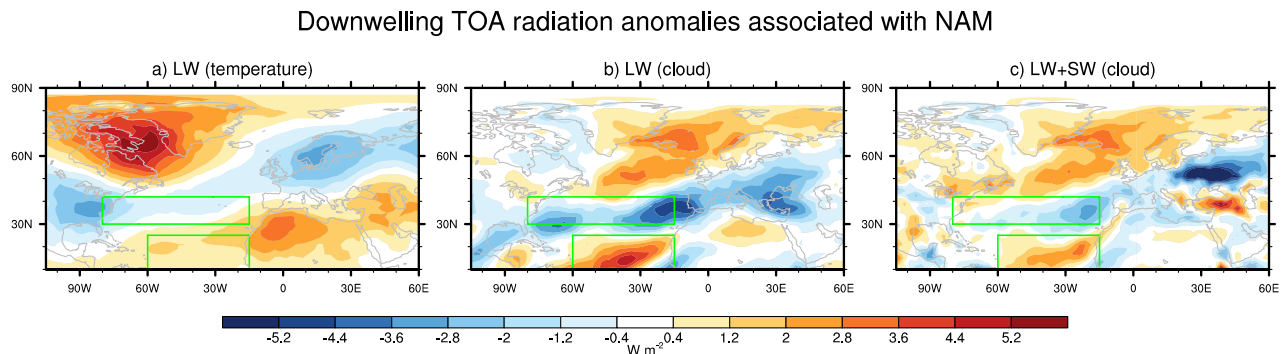


Fig. 4 TOA downwelling radiation anomalies associated with the NAM/NAO contributed from (a) temperature (longwave), (b) cloud (longwave), and (c) cloud (longwave+shortwave). Green boxes indicate example regions where the radiation forcing anomalies due to the changes in temperature and clouds coincide with each other (see text for detail).

4. Concluding remarks

We have explored the signature of the NAM/NAO in the vertical and horizontal distribution of clouds and adjusted CRF in both CloudSat/CALIPSO data and ERA-Interim reanalysis. The positive polarity of the NAM/NAO is marked by coherent and robust changes in cloud incidence that largely mirror its attendant changes in vertical motion. The changes in cloud incidence associated with the NAM/NAO, in turn, lead to marked anomalies in adjusted CRF. Over the North Atlantic, the anomalies in net adjusted CRF are due primarily to changes in the fluxes of longwave radiation, and are comparable in amplitude to the changes in radiative flux due to the NAM/NAO-related temperature anomalies. The primary cloud incidence and adjusted CRF anomalies associated with the NAM/NAO were found to be reproducible in independent data sources and using different analysis techniques (Figure 2e and compare Figure 3b and c).

In the absence of land-sea contrasts, the adjusted CRF anomalies associated with annular variability might be expected to shorten the timescale of the attendant temperature anomalies. For example: Regions of large-scale ascent and cooling are marked by increases in cloud incidence, and the resulting positive anomalies in longwave adjusted CRF should act to shorten the timescale of the negative atmospheric temperature anomalies (e.g., north of 60°N in Figure 1 and 2e).

In the presence of large land-sea contrasts, the temperature anomalies associated with the NAM/NAO are dominated by horizontal temperature advection (as opposed to vertical motion). Over the high latitudes of the North Atlantic, the cloud and temperature radiative forcing anomalies associated with the NAM/NAO do not clearly coincide with each other (compare Figure 4a and 4c). Over the mid/low latitudes of the North Atlantic, the TOA adjusted CRF anomalies generally reinforce those due to the changes in temperature (e.g., see green boxes of Figure 4). Hence over the mid/low latitudes of the North Atlantic, the adjusted CRF should act to shorten the timescale of the mid/low latitude temperature anomalies associated with the NAM/NAO. The importance of cloud and temperature radiative feedbacks in determining the timescale of large-scale atmospheric phenomena will be examined in a companion study.

References

- Bretherton, C. S., M. Widmann, V. P. Dymnikov, J. M. Wallace, and I. Bladé, 1999: The effective number of spatial degrees of freedom of a time-varying field. *J. Climate*, **12**, 1990–2009.
- Huang, Y., and V. Ramaswamy, 2009: Evolution and trend of the outgoing longwave radiation spectrum, *J. Climate*, **22**, 4637–4651, doi:10.1175/2009JCLI2874.1.
- Huang, Y., V. Ramaswamy, and B. Soden, 2007: An investigation of the sensitivity of the clear-sky outgoing longwave radiation to atmospheric temperature and water vapor, *J. Geophys. Res.*, **112**, D05,104, doi:10.1029/2005JD006906.

- Hurrell, J., Y. Kushnir, M. Visbeck, and G. Ottersen, 2003: An Overview of the North Atlantic Oscillation, in *The North Atlantic Oscillation: Climatic Significance and Environmental Impact. Geophys. Monogr. Ser.*, **134**, pp. 1–35, Amer. Geophys. Union, Washington D.C.
- Hurrell, J. W., 1995: Decadal trends in the North Atlantic Oscillation regional temperatures and precipitation. *Science*, **269**, 676–679.
- Li, Y., and D. W. J. Thompson, 2013: The signature of the stratospheric Brewer-Dobson circulation in tropospheric clouds. *J. Geophys. Res.*, **118**, 3486–3494.
- Li, Y., D. W. J. Thompson, G. L. Stephens, and S. Bony, 2014: A global survey of the instantaneous linkages between cloud vertical structure and large-scale climate. *J. Geophys. Res.*, revised.
- Mace, G. G., Q. Zhang, M. Vaughn, R. Marchand, G. Stephens, C. Trepte, and D. Winker, 2009: A description of hydrometeor layer occurrence statistics derived from the first year of merged CloudSat and CALIPSO data. *J. Geophys. Res.*, **114**, D00A26.
- Shell, K. M., J. T. Kiehl, and C. A. Shields, 2008: Using the radiative kernel technique to calculate climate feedbacks in NCAR’s Community Atmospheric Model. *J. Climate*, **21**, 2269–2282.
- Simmons, A., S. Uppala, D. Dee, and S. Kobayashi, 2007: ERA-Interim: New ECMWF reanalysis products from 1989 onwards. *ECMWF Newsletter*, **110**, 25–35, ECMWF, Reading, United Kingdom.
- Soden, B. J., I. M. Held, R. Colman, K. M. Shell, J. T. Kiehl, and C. A. Shield, 2008: Quantifying climate feedbacks using radiative kernels. *J. Climate*, **21**, 3504–3520.
- Stephens, G. L., 2005: Feedbacks in the climate system: A critical review. *J. Climate*, **18**, 237–273.
- Thompson, D. W. J., and J. M. Wallace, 2000: Annular modes in the extratropical circulation. Part I: Month-to-month variability. *J. Climate*, **13**, 1000–1016.
- Verlinden, K. L., D. W. J. Thompson, and G. L. Stephens, 2011: The three-dimensional distribution of clouds over the Southern Hemisphere high latitudes. *J. Climate*, **24**, 5799–5811.